J. Math. Biol. (2007) 55:517–539
DOI 10.1007/s00285-007-0093-7

Mathematical Biology

Steric hindrance effects on surface reactions: applications to BIAcore

David A. Edwards

Received: 28 January 2006 / Revised: 3 April 2007 / Published online: 25 May 2007

Abstract Because surface-volume reactions occur in many biological and industrial processes, understanding the rate of such reactions is important. The BIAcore surface plasmon resonance (SPR) biosensor for measuring rate constants has such a geometry. Though several models of the BIAcore have been presented, few take into account that large ligand molecules can block multiple receptor sites, thus skewing the sensogram data. In this paper some general mathematical principles are stated for handling this phenomenon, and a surface-reaction model is presented explicitly. An integro-partial differential equation results, which can be simplified greatly using perturbation techniques, yielding linear and nonlinear integrodifferential equations. Explicit and asymptotic solutions are constructed for cases motivated by experimental design. The general analysis can provide insight into surface-volume reactions occurring in various contexts. In particular, the steric hindrance effect can be quantified with a single dimensionless parameter.

Keywords Biomolecular reactions · Rate constants · Asymptotics · Integro-differential equations · Steric hindrance effects · BIAcore

Mathematics Subject Classification (2000) 35B20 · 35C15 · 35K60 · 45J05 · 45K05 · 92C45

This work was supported in part by NIGMS Grant 1R01GM067244-01.

D. A. Edwards (✉)
Department of Mathematical Sciences, University of Delaware,
Newark, DE 19716-2553, USA
e-mail: edwards@math.udel.edu

1 Introduction

Many important industrial and biological processes involve the binding of a free-floating reactant (herein termed the *ligand*) to a reactant (the *receptor*) attached to a two-dimensional surface, such as a cell membrane or channel wall. For instance, in the biological realm, models of blood clots treat the vessel as a reacting wall [1,13]. Distamycin-type drugs bind to reacting sites on the surface of a much larger DNA molecule [20]. Immunoglobulins are transmitted to newborns from mother's milk through binding to receptors on intestinal epithelial cells [25]. Antibodies bind to chemokine receptors in the surface-volume geometry [15]. Gene expression is significantly influenced by DNA-protein interactions in these geometries [28]. The transduction of an odor into an electrical signal to the brain is accomplished by the binding of a free-floating molecule to a receptor on a cilium in the nose [19].

On the industrial side, corrosive processes occur in such geometries [14]. In bubble reactors, gas reacts with the liquid which impinges on the bubble surfaces [22].

Understanding such processes requires knowledge of the *rate constants* for any given reaction. Real-time measurements of the binding process can be translated into such parameters given an appropriate mathematical model. One popular device for obtaining such data is the BIAcore, which is a surface plasmon resonance (SPR) device.

The configuration of the BIAcore is described in great detail elsewhere [17,18,21, 28]. We present a brief review for our purposes (see Fig. 1). The BIAcore device is a rectangular channel through which the ligand is convected in the $\tilde{x}$-direction in standard two-dimensional laminar flow from $\tilde{x} = 0$, the inlet position. The receptor is embedded in a thin dextran matrix attached to the ceiling of the channel. An evanescent wave is bounced off the channel ceiling and read by a detector. As the experiment progresses, binding causes refractive changes to the polarized light beam. These changes, when compared to a control state, can be translated into a *sensogram* of the binding [11].

Once a sensogram has been generated, an accurate mathematical model must be used to fit the data and determine the rate constants. Though several models exist, most omit *steric hindrance effects*. These occur when the ligand molecules are large compared to the spacing of the receptors, causing a single binding event to block

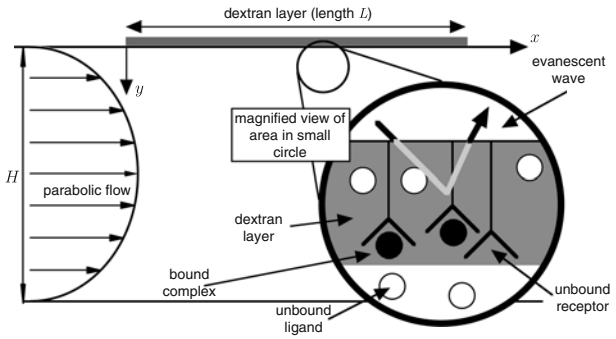

Fig. 1 Schematic of the BIAcore device

multiple receptors. Thus a naïve model which does not include the effect will tend to underestimate the *affinity constant*

$$\tilde{K} = \frac{\tilde{k}_\mathrm{a}}{\tilde{k}_\mathrm{d}}, \tag{1}$$

where $\tilde{k}_\mathrm{a}$ is the association rate constant and $\tilde{k}_\mathrm{d}$ is the dissociation rate constant. This is because receptors which are merely occluded will be counted as receptors which are available, but do not bind because of the kinetics.

The novel approach in this work is to extend previous models of the BIAcore to include steric hindrance effects. In the next section we spell out some general considerations to observe when formulating models of this type. Using some reasonable assumptions, we then specialize to the case where the reaction zone is a surface. This leads to an integro-partial differential equation for the bound state.

Because of the disparate length scales involved, this complicated system may be reduced to the same functional form as the model without steric hindrance effects included. The changes occur in certain dimensionless parameters in the problem. Such a simplification makes it easy to analyze, interpret, and correct errors in the sensogram data due to steric hindrance effects.

Though the results herein are presented in the context of the BIAcore, they have wide applicability. The same occlusion effects can occur on biological surfaces, and information about them can lead to the design of more effective pharmaceuticals. In the industrial realm, such results can help optimize processes by providing upper bounds on the amount of receptor needed to achieve a certain chemical result.

2 Surface steric hindrance model

2.1 General considerations

In this manuscript, we describe the reaction zone in the BIAcore as a surface. This model holds for thin dextran layers or BIAcore products where the receptor is bound directly to the chip surface. The standard surface reaction model can be stated as follows:

$$\frac{\partial \tilde{B}}{\partial \tilde{t}} = \tilde{k}_\mathrm{a}(R_\mathrm{T} - \tilde{B})\tilde{C}(\tilde{x}, 0, \tilde{t}) - \tilde{k}_\mathrm{d}\tilde{B}, \qquad 0 \le \tilde{x} \le L, \tag{2}$$

where $\tilde{B}$ is the concentration of bound ligand on the surface, $\tilde{C}$ is the concentration of the unbound ligand in the flow, L is the length of the channel, and R_T is the total number of receptors. Though the receptor density may initially be nonuniform [16,24] in this work we take it to be uniform, since the error introduced from such an assumption is small [10]. The parenthetical term in Eq. (2) is the number of receptors available for binding, given that each binding site takes up just one receptor.

To include steric hindrance effects, we note that if the ligand molecule is large, when it binds with one site it may occlude other neighboring sites. Therefore,

we replace Eq. (2) with the following:

$$\frac{\partial \tilde{B}}{\partial \tilde{t}} = \tilde{k}_{\mathrm{a}}\{R_{\mathrm{T}} - \mathcal{S}[\tilde{B}]\}\tilde{C}(\tilde{x}, 0, \tilde{t}) - \tilde{k}_{\mathrm{d}}\tilde{B}, \tag{3}$$

where $\mathcal{S}[\tilde{B}]$ is a *steric hindrance operator* that measures how many receptor sites on average are occluded by a single binding event. Clearly $\mathcal{S}[\tilde{B}] \geq \tilde{B}$.

This new operator formulation for steric hindrance effects is of course quite general. To specialize to a form which we can actually solve, we introduce the following additional assumptions:

1. Receptor sites are considered to be points, spaced evenly on the sensor surface at a distance d_{r} from one another, where the subscript "r" stands for "receptor".
2. Ligand molecules are considered to have only one specific binding site centered in the structure. The structure is considered to be of characteristic size d_{l}, where the subscript "l" stands for "ligand". In practice, d_{l} will be taken as twice the Stokes radius.
3. As the experiment progresses, molecules will form an optimal packing arrangement. This is probably the most controversial assumption, though in the next section we describe situations where this can occur. In any event, this assumption will provide a lower bound on the effect (since more disordered configurations will occlude more reacting sites).
4. In order to transition from discrete receptor sites on individual molecules to the continuum approximation in Eq. (3), we rely upon the fact that there is a third $\tilde{z}$-direction normal to the flow. This direction is always averaged away in the measurements, and hence $\tilde{B}$ at some specified $\tilde{x}_*$ can be thought of as a proportion of receptor sites at $(\tilde{x}_*, \tilde{z})$ which have been bound, thus yielding after some manipulation an area concentration.
5. Because the ligand molecules are no longer considered to be points, we identify the position of a ligand molecule by the position of its receptor site. In other words, as described above, $\tilde{C}(\tilde{x})$ would be the concentration of molecules (averaged over $\tilde{z}$) which have their receptor sites at $\tilde{x}$.

Each of the above assumptions may introduce errors into our solution. Fortunately, the BIAcore signal is averaged over a finite *scanning range*:

$$\bar{\tilde{B}}(t) = \frac{1}{\tilde{x}_{\max} - \tilde{x}_{\min}} \int_{\tilde{x}_{\min}}^{\tilde{x}_{\max}} \tilde{B}(\tilde{x}, t)\, \mathrm{d}\tilde{x}, \tag{4}$$

where $\tilde{x}_{\min}$ and $\tilde{x}_{\max}$ are bounded away from the ends of the device. Since none of the errors in the assumptions would seem to introduce a definite directional bias, the averaging process should minimize their effect on the solution.

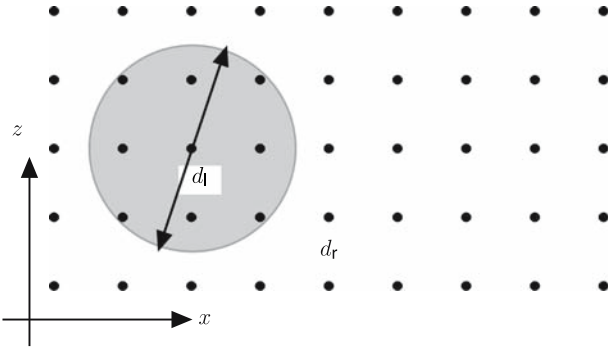

Fig. 2 Schematic of two-dimensional model, top view

2.2 The two-dimensional case

Figure 2 shows a view looking down at the reacting surface. The receptor sites are indicated by black dots, and the ligand molecule is represented as a grey disk. The binding site is at the center of the disk, which identifies the position of the ligand molecule. The disk can be thought of as the projection (or "shadow") of a three-dimensional spherical molecule onto the two-dimensional reacting surface. Thus disks cannot overlap.

Figure 2 shows a single binding event that will render unavailable all receptors within a *radius* d_l from the binding site. Receptors within a radius $d_l/2$ are directly occluded by the ligand molecule, while receptors in the annulus between radii $d_l/2$ and d_l are unavailable due to overlap effects. We expect $\mathcal{S}[\tilde{B}]$ to be linear in $\tilde{B}$, since (considering the averaging in the $\tilde{z}$-direction) we expect twice as many bound states to occlude twice as many molecules. This discussion motivates the following model for $\mathcal{S}$:

$$\mathcal{S}[\tilde{B}](\tilde{x},\tilde{z},\tilde{t}) = \mathcal{S}_0 \int_{-d_l}^{d_l} \int_{-\sqrt{d_l^2-\tilde{x}'^2}}^{\sqrt{d_l^2-\tilde{x}'^2}} \tilde{B}(\tilde{x}+\tilde{x}',\tilde{z}+\tilde{z}',\tilde{t})\,\mathrm{d}\tilde{z}'\,\mathrm{d}\tilde{x}', \tag{5}$$

where $\mathcal{S}_0$ is a normalization factor.

Consider the aspect ratio $\epsilon = H/w$, where H is the height of the channel and w its width. From the values in the Appendix, we have that $\epsilon \ll 1$, so to leading order $\tilde{B}$ is also independent of $\tilde{z}$, and hence from Eq. (3) we conclude that $\tilde{B}$ will always be independent of $\tilde{z}$.

Thus we may easily compute the inner integral in Eq. (5) to obtain

$$\mathcal{S}[\tilde{B}](\tilde{x},\tilde{t}) = \mathcal{S}_0 \int_{-d_l}^{d_l} 2\sqrt{d_l^2-\tilde{x}'^2}\,\tilde{B}(\tilde{x}+\tilde{x}',\tilde{t})\,\mathrm{d}\tilde{x}'. \tag{6}$$

In order to calculate $\mathcal{S}_0$, it is convenient to scale the problem, which for the physical variables we do in the normal way:

$$x = \frac{\tilde{x}}{L}, \qquad B(x,t) = \frac{\tilde{B}(\tilde{x},\tilde{t})}{R_\mathrm{T}}. \tag{7a}$$

The importance of this scaling is that the dimensionless B now represents the percentage of receptor sites bound. However, for the dummy variable it is more convenient to scale by the diameter of the ligand molecule:

$$x' = \frac{\tilde{x}'}{d_\mathrm{l}} \quad \Longrightarrow \quad \frac{\tilde{x}+\tilde{x}'}{L} = x + \delta x', \qquad \delta = \frac{d_\mathrm{l}}{L}. \tag{7b}$$

Substituting Eqs. (7a) and (7b) into Eq. (6), we obtain

$$\mathcal{S}[B](\tilde{x},\tilde{t}) = 2R_\mathrm{T}\mathcal{S}_0 d_\mathrm{l}^2 \int_{-1}^{1} \sqrt{1-x'^2}\, B(x+\delta x',t)\,\mathrm{d}x'. \tag{8}$$

For the other terms in Eq. (3), we note from previous work [6] that the area of interest is a small boundary layer above the reacting surface. The appropriate time scale is the forward reaction time scale. Therefore, we let

$$t = \tilde{k}_\mathrm{a} C_\mathrm{u} \tilde{t}, \qquad y = \mathrm{Pe}^{1/3}\frac{\tilde{y}}{H}, \qquad \tilde{C}(\tilde{x},\tilde{y},\tilde{t}) = C_\mathrm{u}[1-\mathrm{Da}C(x,y,t)], \tag{9a}$$

where $\tilde{y}$ measures height above the reacting surface and C_u is the upstream inlet concentration. Here Da is the *Damköhler number*, given by

$$\mathrm{Da} = \frac{\tilde{k}_\mathrm{a} R_\mathrm{T}}{\tilde{D}/(H\mathrm{Pe}^{-1/3})} = \frac{\text{reaction ``velocity''}}{\text{diffusion ``velocity'' in diffusive boundary layer}}, \tag{9b}$$

where $\tilde{D}$ is the diffusion coefficient of the ligand molecules in the flow. Here Pe is the Péclet number, given by

$$\mathrm{Pe} = \frac{H^2/\tilde{D}}{L/V} = \frac{\text{characteristic diffusion time in flow}}{\text{characteristic convection time in flow}}, \tag{9c}$$

where V is a typical velocity scale.

Substituting Eqs. (7)–(9) into Eq. (3), we obtain

$$\frac{\partial B}{\partial t} = \left[1 - 2\mathcal{S}_0 d_\mathrm{l}^2 \int_{-1}^{1} \sqrt{1-x'^2}\, B(x+\delta x',t)\,\mathrm{d}x'\right][1-\mathrm{Da}C(x,0,t)] - KB, \tag{10a}$$

$$K = \frac{\tilde{K}}{C_\mathrm{u}}. \tag{10b}$$

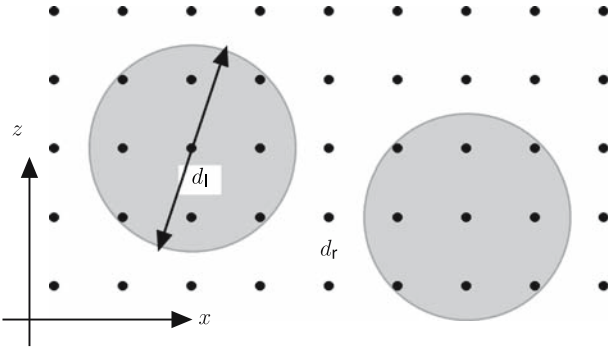

Fig. 3 Poorly packed configuration

2.3 Determining the normalization factor

To determine $\mathcal{S}_0$, we consider a nearly irreversible reaction by taking $K \to 0$. Since the backwards reaction proceeds slowly, it eliminates poorly packed configurations as in Fig. 3, working only to distribute the receptors uniformly so Assumption 3 above holds.

We also examine the steady state of the system, starting with C. At steady state the reaction stops, and the ligand concentration reverts to the inlet concentration C_u, which means that $C_s = 0$, where the subscript "s" refers to "steady state". (More details of this derivation may be found in [7].)

Thus in the small-K limit, the steady state of Eq. (10a) satisfies

$$2\mathcal{S}_0 d_l^2 \int_{-1}^{1} \sqrt{1 - x'^2} B_s(x + \delta x')\, dx' = 1. \tag{11}$$

Equation (11) is the mathematical statement of the chemical reality that if the reaction is irreversible, at steady state all the receptors must be either bound or occluded.

Since we are working in the continuous limit of averaging with perfect distribution of binding sites, B_s will be uniform. In addition, we note from the schematic in Fig. 2 that $d_l \approx 2d_r\sqrt{2}$, and (neglecting edge effects) roughly $1/8 = (d_r/d_l)^2$ of the receptors would be occluded if the disks were packed optimally. So as long as $d_l \geq d_r$, the proportion of receptors bound at steady state is given by $(d_r/d_l)^2$.

For reasons that will become clear later, it is easier to work with the inverse of this quanitity, which we denote by p. So we have $B_s = p^{-1}$, where

$$p = \max\left\{\frac{d_l^2}{d_r^2}, 1\right\}. \tag{12}$$

Here we use the maximum to take into account the case where the ligand size is smaller than the receptor spacing.

In order to apply our theory to a particular experiment, we must know the value of p. d_l is readily obtainable from the Stokes radius for the ligand molecule, which can be estimated using gel filtration techniques [12] or size exclusion chromatography [27]. For d_r, we note that the area density of molecules is just given by $N R_\mathrm{T}$, where N is Avogadro's number. Then the average area occupied per molecule is just $(N R_\mathrm{T})^{-1}$. Assuming a uniform square lattice, this means that the spacing between molecules is just the square root of that quantity, so

$$d_\mathrm{r} = (N R_\mathrm{T})^{-1/2} \qquad \Longrightarrow \qquad p = \max\{d_\mathrm{l}^2 N R_\mathrm{T}, 1\}. \tag{13}$$

Thus p is directly proportional to R_T and hence can be controlled in an experiment.

Substituting our expression for B_s into Eq. (11), we obtain a value for $\mathcal{S}_0$. Substituting this result into Eq. (8), we obtain

$$\mathcal{S}[B](x,t) = \frac{2R_\mathrm{T}p}{\pi} \int_{-1}^{1} \sqrt{1-x'^2}\, B(x+\delta x', t)\, \mathrm{d}x'. \tag{14}$$

2.4 Additional considerations

Substituting our form for $\mathcal{S}_0$ into Eq. (10a) yields the full evolution equation for the hindered case:

$$\frac{\partial B}{\partial t} = \left[1 - \frac{2p}{\pi} \int_{-1}^{1} \sqrt{1-x'^2}\, B(x+\delta x', t)\, \mathrm{d}x'\right] [1 - \mathrm{Da} C(x,0,t)] - K B. \tag{15}$$

One can envision a situation where a ligand molecule binds very close to the end of the receptor surface, and hence the entire disk surface need not be considered in the occlusion process. Fortunately, because the scanning range is bounded away from the ends of the device, such a situation would not affect the analysis.

To complete our model, we need several more pieces of information. First, we must have an initial condition for B, which we assume uniform (It will be zero for an association experiment, and the steady state otherwise). Thus we have

$$B(x,0) = B_\mathrm{i}, \tag{16}$$

where B_i is considered to be an $O(1)$ constant.

We also need an expression for C. Since steric hindrance effects do not affect the transport of ligand, we may quote the result from [9], which considers the surface reaction case:

$$C(x,0,t) = \frac{1}{3^{1/3}\Gamma(2/3)} \int_0^x \frac{\partial B}{\partial t}(x-x', t) \frac{\mathrm{d}x'}{x'^{2/3}}. \tag{17}$$

This result is obtained using the same sort of geometry and flux balance as in the Ward–Tordai model [26,29]. In particular, there is a thin boundary layer above the reacting surface which is taken to be semi-infinite, and diffusive flux normal to the surface is balanced with the increase in B. However, it differs from the standard Ward–Tordai model in that it uses an advection–diffusion equation for C, incorporating flow in the transverse direction.

Since C as scaled represents the deviation from the inlet value, Eq. (17) states that this deviation at position x is simply the accumulation of depletion effects upstream ($0 < x' < x$), modified by an integral kernel that takes into account flow effects.

From the Appendix we have that $\delta \ll 1$. Thus expanding the integral in Eq. (15) for small δ, we obtain

$$\frac{\partial B}{\partial t} = \left(1 - pB + \frac{\delta^2 p}{8}\frac{\partial^2 B}{\partial x^2}\right)[1 - \mathrm{Da}C(x, 0, t)] - KB. \tag{18}$$

3 Small Da

3.1 Association experiment

Scientists attempt to minimize the effects of transport on their experiments. This corresponds to the mathematical case of small Da. Therefore, we introduce the following perturbation series in Da for B:

$$B(x, t) = B_0(x, t) + \mathrm{Da}B_1(x, t) + o(\mathrm{Da}). \tag{19}$$

Motivated by the form of Eq. (18), we assume that $\delta^2 = O(\mathrm{Da})$ to obtain a dominant balance. Substituting Eq. (19) into Eqs. (18) and (16) and keeping terms to leading two orders, we have

$$\frac{\partial B_0}{\partial t} + \alpha B_0 = 1, \quad B_0(x, 0) = B_\mathrm{i}; \qquad \alpha = K + p, \tag{20a}$$

$$\frac{\partial B_1}{\partial t} + \alpha B_1 = \frac{\delta^2 p}{8\mathrm{Da}}\frac{\partial^2 B_0}{\partial x^2} - C_\mathrm{f}(x, 0, t)(1 - pB_0), \quad B_1(x, 0) = 0. \tag{20b}$$

The only difference between Eq. (20a) and the leading-order equation in previous studies is the redefinition of the parameter α [5]. Since this is the only change, we can easily see how neglecting steric hindrance can affect our results (at least to leading order). In particular, if we ignore steric hindrance effects when analyzing our data, then the estimated value deviates from the true value in the following way:

$$K_\mathrm{estimated} = K_\mathrm{true} + p - 1. \tag{21}$$

Therefore, the absolute error will be most apparent when K_true is small. Since K depends on C_u and p depends on R_T, that means this error is controllable in an experiment, even if the exact diameter of the ligand molecule is unknown.

Solving Eq. (20a), we obtain

$$B_0(x,t) = \frac{1-\mathrm{e}^{-\alpha t}}{\alpha} + B_\mathrm{i}\mathrm{e}^{-\alpha t}. \tag{22}$$

Note from Eq. (22) that the true physical time scale for the problem is essentially measured as a reciprocal of α.

There are several ramifications of the fact that B_0 is independent of x. First, the measured quantity indicated in Eq. (4) is simply given by B_0 itself:

$$\bar{B}_0(t) = B_0 = \frac{1-\mathrm{e}^{-\alpha t}}{\alpha} + B_\mathrm{i}\mathrm{e}^{-\alpha t}. \tag{23}$$

Second, to leading order we may factor $\partial B/\partial t$ from the integrand of Eq. (17) to obtain

$$C(x,0,t) = \frac{\mathrm{d}B_0}{\mathrm{d}t}h(x), \qquad h(x) = \frac{3^{2/3}x^{1/3}}{\Gamma(2/3)}. \tag{24}$$

Third, since B_0 is independent of x, the p term in Eq. (20b) vanishes. Hence, any change to the solution because of such nonuniformities must occur at $O(\mathrm{Da}^2)$.

Substituting this result, Eqs. (22), and (24) into Eq. (20b) and solving, we have the following:

$$B_1 = \left[\frac{(\mathrm{e}^{-\alpha t}-1)p\chi}{\alpha} - Kt\right]\frac{\chi\mathrm{e}^{-\alpha t}h(x)}{\alpha}, \quad \chi = 1-\alpha B_\mathrm{i}. \tag{25}$$

Note that this expression is similar to the result in [5], except for the additional p coefficient. Then averaging to obtain a result consistent with the BIAcore signal, we have

$$\bar{B}_1 = \left[\frac{(\mathrm{e}^{-\alpha t}-1)p\chi}{\alpha} - Kt\right]\frac{\chi\mathrm{e}^{-\alpha t}\bar{h}}{\alpha}, \qquad \bar{h} = \frac{3^{5/3}\left(x_\mathrm{max}^{4/3}-x_\mathrm{min}^{4/3}\right)}{4\Gamma(2/3)(x_\mathrm{max}-x_\mathrm{min})}, \tag{26}$$

where we have used Eq. (24).

Note that Eq. (26) has a term that behaves like $t\mathrm{e}^{-\alpha t}$, which is similar in form to a secular term in a two-timing problem. Of course, due to the fact that B_0 approaches an $O(1)$ steady state, $\mathrm{Da}B_1 \ll B_0$ for all t, and so technically the expansion does not fail at this order. Nevertheless, this is still a secular form. The standard way to fix such a problem is to introduce a multiple-scale expansion, as in [8]. This reference shows that though it is possible to construct such an expansion, it will not be illuminating.

3.2 Effective rate constant solution

Instead, we restate our results in the *effective rate constant* (ERC) context, which presents a simple ODE model for the actual sensogram data $\bar{B}$. Substituting Eq. (24)

Table 1 Parameters for Figs. 4–7 [6]

Parameter	Value	Parameter	Value
B_i	0	t	$10^{-3}\,\tilde{t}/\mathrm{s}$
C_u (mol/cm^3)	10^{-11}	x_max	7.92×10^{-1}
Da	10^{-1}	x_min	2.08×10^{-1}
$\tilde{k}_\mathrm{a}$(cm^{3}mol^{-1}s^{-1})	10^8		

into Eq. (18), we have

$$\frac{\partial B}{\partial t} = \left(1 - pB + \frac{\delta^2 p}{8}\mathrm{Da}\frac{\partial^2 B_1}{\partial x^2}\right)\left[1 - \mathrm{Da}\frac{\mathrm{d}B_0}{\mathrm{d}t}h(x)\right] - KB + O(\mathrm{Da}^2).$$

Since B_0 is independent of x, we may manipulate the above and average it over the scanning range to obtain

$$\frac{\mathrm{d}\bar{B}}{\mathrm{d}t} = \frac{1 - \alpha\bar{B}}{1 + \mathrm{Da}(1 - p\bar{B})\bar{h}} + O(\mathrm{Da}^2), \tag{27}$$

where we have used our assumption about the size of δ^2 to construct our order estimate. Note that with the exception of the redefinition of α and the new p term, this is exactly the same result as obtained in the case without steric hindrance [6].

We now present some graphs of our results. As discussed above, the effect of $p \neq 1$ will be different depending on the size of K. Therefore, we present two sets of graphs; one for $K = 1$ (the default value used for previous papers, cf. [7]) and one for K large. Note that this involves varying $\tilde{k}_\mathrm{d}$, since the other parameters are fixed in Table 1 above. From a physical point of view, we vary p simply by varying d_l; we keep R_T fixed to fix d_r.

Figure 4 shows the solution of the ERC equation with $K = 1$ (used in previous work) with various p. Because of the form of Eq. (20a), the graphs for $K < 1$ are similar, since in both cases the variation due to p dominates. Note that both the maximum value attained and the time scale needed to reach the maximum decreases as p^{-1}.

Figure 5 shows the same graphs as in Fig. 4, but for $K = 10$. Since K is now larger, the effect of increasing p is not as pronounced, though it is still significant.

3.3 Dissociation experiment

In a typical BIAcore experiment, a dissociation run is initiated once the association run has reached steady state. From Eq. (17) we see that as $t \to \infty$, $C(x, 0, t) \to 0$, so using the same arguments in Sect. 3.1, one can determine that the steady state of Eq. (15) is

$$B_\mathrm{s} = \frac{1}{\alpha}. \tag{28}$$

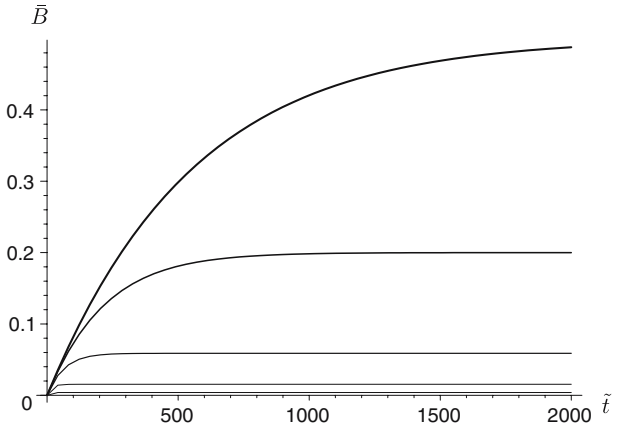

Fig. 4 Solution of Eq. (27) with $K = 1$ and (in decreasing order of thickness) $p = 1, 2, 4, 8$, and 16

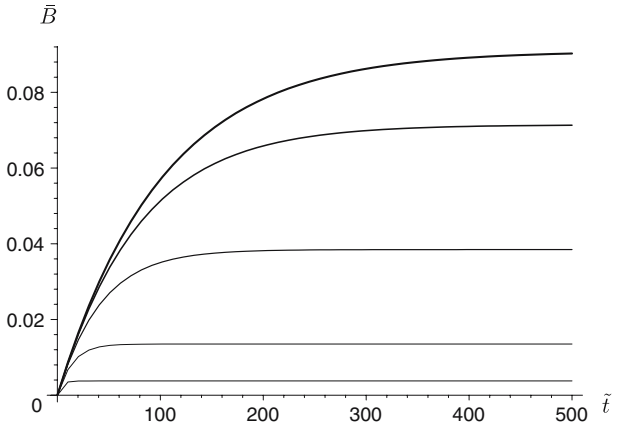

Fig. 5 Solution of Eq. (27) with $K = 10$ and (in decreasing order of thickness) $p = 1, 2, 4, 8$, and 16

Equation (28) provides the initial condition for the dissociation problem, and hence we are justified by always taking the initial condition for B to be spatially uniform, as postulated in Sect. 2.4.

In addition, the ligand concentration is shut off, so the equation analogous to Eq. (15) is

$$\frac{\partial B}{\partial t} = \left[1 - \frac{2p}{\pi}\int_{-1}^{1}\sqrt{1-x'^2}B(x+\delta x', t)\,\mathrm{d}x'\right][-\mathrm{Da}C(x,0,t)] - KB. \quad (29)$$

Expanding Eq. (29) for small δ and Da, we obtain, to leading two orders,

$$\frac{\partial B_0}{\partial t} + KB_0 = 0, \quad B_0(x,0) = \alpha^{-1}, \tag{30a}$$

$$\frac{\partial B_1}{\partial t} + KB_1 = -(1 - pB_0)C(x,0,t), \quad B_1(x,0) = 0. \tag{30b}$$

Solving Eq. (30a), we have the following:

$$B_0(x,t) = \bar{B}_0(t) = \frac{\mathrm{e}^{-Kt}}{\alpha}. \tag{31}$$

Since Eq. (24) does not change, we may substitute it and Eq. (31) into Eq. (30b) to obtain

$$B_1 = \frac{K}{\alpha}\left[t + \frac{p(\mathrm{e}^{-Kt} - 1)}{K\alpha}\right] h(x)\mathrm{e}^{-Kt}. \tag{32}$$

Note this expression is similar to [8, Eq. (3.21b)] (where no steric hindrance effects are present), except for the addition of the new parameter p. Then averaging, we have

$$\bar{B}_1 = \frac{K}{\alpha}\left[t + \frac{p(\mathrm{e}^{-Kt} - 1)}{K\alpha}\right] \bar{h}\mathrm{e}^{-Kt}, \tag{33}$$

where $\bar{h}$ is given in Eq. (26). Note that we have the same secularity problem, more obvious now because the steady state is now zero, so the second term really is larger than the first.

The effective rate constant work may also be replicated for the dissociation case. Substituting Eq. (24) into Eq. (29) and expanding for small δ yields the following:

$$\frac{\mathrm{d}\bar{B}}{\mathrm{d}t} = \frac{-K\bar{B}}{1 + \mathrm{Da}(1 - p\bar{B})\bar{h}} + O(\mathrm{Da}^2). \tag{34}$$

in an analogous way to that used to derive Eq. (27).

Figures 6 and 7 are analogous to Figs. 4 and 5, but for the dissociation case. As in the previous subsection, the effect of varying p is most pronounced when K is small.

4 Moderate Da

Occasionally, the material parameters are such that Da cannot be forced small. This occurs when the reaction is very fast, or when R_T must be set large so that the sensogram signal swamps any noise in the measurements.

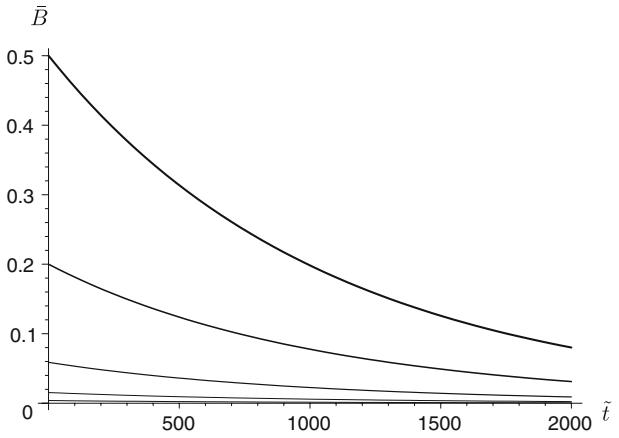

Fig. 6 Solution of Eq. (34) with $K = 1$ and (in decreasing order of thickness) $p = 1, 2, 4, 8$, and 16

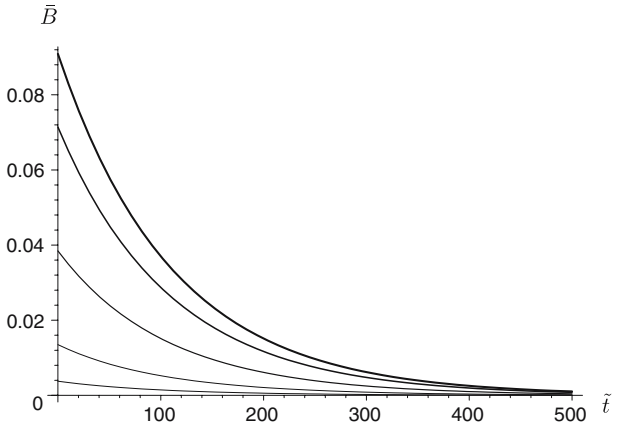

Fig. 7 Solution of Eq. (34) with $K = 10$ and (in decreasing order of thickness) $p = 1, 2, 4, 8$, and 16

4.1 Association experiment

Substitution of Eq. (17) into Eq. (18) yields a nonlinear problem. Therefore we are forced to resort to small-time asymptotics by assuming a solution of the form

$$B(x,t) = B_{\mathrm{i}} + \beta(x)t + o(t). \tag{35}$$

Substituting Eqs. (17) and Eq. (35) into Eq. (18) and rearranging, we have, to leading order in t,

$$\chi - \beta = \frac{\mathrm{Da}(1 - pB_{\mathrm{i}})}{3^{1/3}\Gamma(2/3)} \int_0^x \beta(x - x', t) \frac{\mathrm{d}x'}{x'^{2/3}}. \tag{36}$$

By defining

$$\mathcal{I}[\beta; x] \equiv \int_0^x \beta(x')\,\mathrm{d}x', \tag{37}$$

we may write the average in dimensional terms with the aid of Eq. (9a):

$$\begin{aligned} \bar{B}(\tilde{t}) &\sim B_\mathrm{i} + S\tilde{t}, \quad \tilde{t} \to 0, \\ S &= \frac{\tilde{k}_\mathrm{a} C_\mathrm{u}\{\mathcal{I}[\beta; x_\mathrm{max}] - \mathcal{I}[\beta; x_\mathrm{min}]\}}{x_\mathrm{max} - x_\mathrm{min}}. \end{aligned} \tag{38}$$

Using Laplace transform techniques, one finds that $\mathcal{I}$ for the solution of Eq. (36) is

$$\mathcal{I}[\beta; x] = \frac{\chi \mathrm{e}^{-\nu_\mathrm{a} x}}{\nu_\mathrm{a}} \left[\mathrm{e}^{\nu_\mathrm{a} x} - 1 - |P(4/3, -\nu_\mathrm{a} x)| + |P(5/3, -\nu_\mathrm{a} x)|\right], \tag{39}$$

$$\nu_\mathrm{a} = \frac{1}{3}\left[\frac{\mathrm{Da}(1 - pB_\mathrm{i})\Gamma(1/3)}{\Gamma(2/3)}\right]^3, \tag{40a}$$

where the subscript "a" refers to "association experiment" and P is the normalized lower incomplete gamma function whose definition is

$$P(m/3, -\nu_\mathrm{a} x) = \frac{\gamma(m/3, -\nu_\mathrm{a} x)}{\Gamma(m/3)}. \tag{40b}$$

This is simply the result without steric hindrance effects [5] with new values of χ and ν_a.

In order to calculate both rate constants, we proceed as follows. By simply running the experiment to steady state, we obtain an estimate for α, and hence K. Next we construct a linear fit to our small-time data. Once we have that slope S, we solve Eq. (38) to obtain $\tilde{k}_\mathrm{a}$. It is important to note that the relationship is not linear, since S also depends on $\tilde{k}_\mathrm{a}$ through the parameter Da. Then using our value for K, we may calculate $\tilde{k}_\mathrm{d}$.

p enters into Eq. (39) only as a coefficient of B_i (both in χ and ν_a). Since in the association problem $B_\mathrm{i} = 0$, p does not play a role. Physically, since we are examining short-time solutions, there hasn't been enough time for site exclusion to have a significant effect.

Thus our solutions behave exactly the same as in [5]. In particular, we quote the small- and large-$\tilde{k}_\mathrm{a}$ asymptotes, which correspond to slow and fast reactions. When the reaction is slow, we obtain

$$S \sim \tilde{k}_\mathrm{a} C_\mathrm{u} \chi, \qquad \tilde{k}_\mathrm{a} \to 0. \tag{41}$$

Equation (41) merely shows that if there is no forward reaction ($\tilde{k}_\mathrm{a} = 0$), then there will be no change in the bound concentration from the initial state ($S = 0$).

For the large $\tilde{k}_\mathrm{a}$ asymptote, we have that

$$S \sim \frac{3^{4/3} C_\mathrm{u} V^{1/3} \tilde{D}^{2/3} \left(x_\mathrm{max}^{2/3} - x_\mathrm{min}^{2/3}\right)}{2\Gamma(1/3) R_\mathrm{T} L^{1/3} H^{1/3} (x_\mathrm{max} - x_\mathrm{min})}, \qquad \tilde{k}_\mathrm{a} \to \infty. \tag{42}$$

Equation (42) simply states that as the reaction speed becomes infinitely fast, the sensogram data will approach a finite slope, as transport becomes the limiting factor.

4.2 Dissociation experiment

We conclude with a discussion of the dissociation case. As stated previously, the initial condition here is the steady state from the association problem given in Eq. (28). Thus Eq. (30a) holds even if we drop the subscript 0. In addition, the leading-order concentration is now 0, not 1. Hence the equation analogous to Eq. (36) becomes

$$\beta + \frac{K}{\alpha} = -\frac{\mathrm{Da}(K/\alpha)}{3^{1/3}\Gamma(2/3)} \int_0^x \beta(x - x', t) \frac{\mathrm{d}x'}{x'^{2/3}}. \tag{43}$$

Examination of Eq. (43) shows that the only structural change we have made is to replace χ by $-K/\alpha$ on the left-hand side. All the other changes are simply changes to the parameters. Thus we have that $\mathcal{I}$ is given by

$$\mathcal{I}[\beta; x] = -\frac{K \mathrm{e}^{-\nu_\mathrm{d} x}}{\nu_\mathrm{d} \alpha} \left[\mathrm{e}^{\nu_\mathrm{d} x} - 1 - |P(4/3, -\nu_\mathrm{d} x)| + |P(5/3, -\nu_\mathrm{d} x)|\right], \tag{44a}$$

$$\nu_\mathrm{d} = \frac{1}{3}\left[\frac{\mathrm{Da}(K/\alpha)\Gamma(1/3)}{\Gamma(2/3)}\right]^3, \tag{44b}$$

where the subscript "d" refers to "dissociation experiment". Note that the slope is now negative, as is correct for our dissociation problem.

Our solution depends on p through α, which appears in the initial condition and in ν. Since the rate constant $\tilde{k}_\mathrm{a}$ also appears in ν, we fix a value of $\tilde{k}_\mathrm{d}$, not K, to evaluate the steric hindrance effects in this case. Thus we will choose a series of $\tilde{k}_\mathrm{d}$ values to see how the solution depends on p for each one. We expect the results to be most pronounced at small values of K, which correspond to small values of $\tilde{k}_\mathrm{d}$. The first value we choose is the one in [7]:

$$\tilde{k}_\mathrm{d} = \frac{8.9 \times 10^{-3}}{\mathrm{s}}. \tag{45}$$

The other parameters listed are in Table 2; k is a variable defined for convenience.

Figure 8 shows the graph of $|S|$ versus $\tilde{k}_\mathrm{on}$ for various values of p. Note that increasing p reduces the initial speed of dissociation, with the most dramatic trends occurring as $\tilde{k}_\mathrm{a}$ gets large, since with larger $\tilde{k}_\mathrm{a}$, the inherent time scale of our problem decreases.

Table 2 Additional parameter values for Figs. 8, 9 [6]

Parameter	Value	Parameter	Value
D (cm^2/s)	2.8×10^{-7}	Pe	3.71×10^2
H (cm)	5×10^{-3}	R_T(mol/cm^2)	10^{-12}
k	$10^{-9} k_a$ mol $\cdot$ s/cm^3	V (cm/s)	1
L (cm)	2.4×10^{-1}		

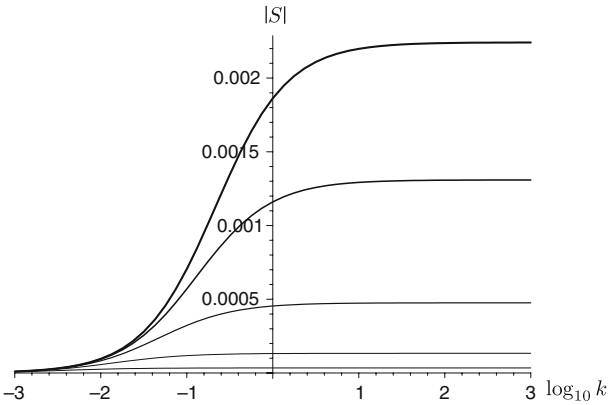

Fig. 8 $|S|$ versus $\log_{10} k$ with $\tilde{k}_d$ as defined in Eq. (45) and (in decreasing order of thickness) $p = 1, 2, 4, 8$, and 16

To obtain the small-$\tilde{k}_a$ asymptote of the graph, we first note that

$$\lim_{\tilde{k}_a \to 0} \frac{K}{\alpha} = 1, \tag{46}$$

since with $\tilde{k}_d$ fixed, $\tilde{k}_a \to 0$ forces $K \to \infty$. Thus from Eq. (44b) we see that small $\tilde{k}_a$ will correspond to small ν_d and we can use the asymptote from the association case, simply replacing χ by $-K/\alpha$ in Eq. (41), which yields

$$S \sim -\tilde{k}_a C_u, \qquad \tilde{k}_a \to 0. \tag{47}$$

This result is independent of p. The effects of blocking from the association experiment are built into the initial condition. Hence for small time, any blocking effects from rebinding in the dissociation experiment have not yet had an opportunity to develop.

Next we examine the large-$\tilde{k}_a$ asymptote. First, we derive the following useful limit:

$$\lim_{\tilde{k}_a \to \infty} \nu_d = \frac{1}{3\mathrm{Pe}} \left[\frac{\Gamma(1/3)}{\Gamma(2/3)} \frac{\tilde{R}_T H}{\tilde{D}} \frac{\tilde{k}_d}{C_u p} \right]^3. \tag{48}$$

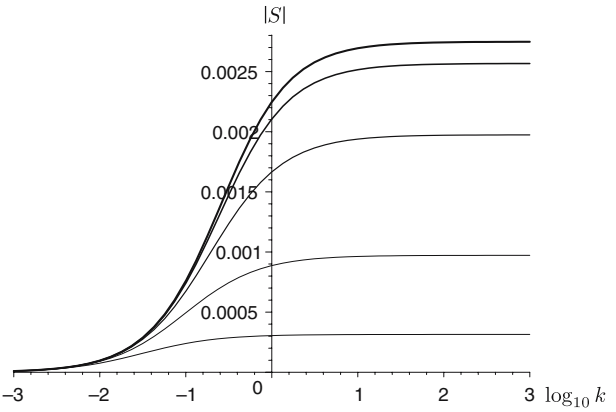

Fig. 9 $|S|$ vs $\log_{10} k$ with $\tilde{k}_{\mathrm{d}}$ as defined in Eq. (49) and (in decreasing order of thickness) $p = 1, 2, 4, 8,$ and 16

Therefore, just as in [7], ν_{d} no longer becomes unbounded as $\tilde{k}_{\mathrm{a}}$ does. We do see that its final value decays as p^{-3}. Therefore, larger values of p will correspond to smaller values of ν_{d}. This will drive down the value of the asymptote, as shown in Fig. 8.

As in Sect. 3.3, we now wish to change $\tilde{k}_{\mathrm{d}}$ and see how the variance with p changes. In that section, we increased K by a factor of 10. Therefore, to achieve the same result in this context, we increase $\tilde{k}_{\mathrm{d}}$ by a factor of 10:

$$\tilde{k}_{\mathrm{d}} = \frac{8.9 \times 10^{-2}}{\mathrm{s}} \tag{49}$$

and display the results in Fig. 9. Note that just as in Sect. 3.3, the effects of p are mitigated with increasing $\tilde{k}_{\mathrm{d}}$. This is because dissociation plays a larger role in the reaction, and dissociation is unaffected by steric hindrance.

5 Discussion and further research

Many biological and industrial processes include surface-volume reactions. Understanding the rates of the underlying kinetic processes is thus essential. The BIAcore SPR device provides an excellent way to obtain real-time observations of binding processes, but such data is useless for parameter estimation without the necessary mathematical models to interpret it. Though many models ignore this, when ligand molecules are larger than the spacing of the receptor molecules on the surface, a single binding event can occlude multiple binding sites. Without taking this steric hindrance effect into account, one will obtain inaccurate overestimates of the affinity constant $\tilde{K}$.

We presented a general model to handle such effects in Sect. 2.1. Though we made some crude simplifying assumptions to obtain a tractable set of equations, the errors we make should be unbiased. Thus the fact that the BIAcore signal averages the binding along the channel length should reduce any errors associated with these assumptions.

When applied to the two-dimensional surface reaction case, the result is an integro-partial differential equation involving the operator $\mathcal{S}[B]$, which models the effect of binding on neighboring receptor sites. Fortunately, due to the large discrepancy in size between the molecules and the channel (captured in the dimensionless parameter δ), the system simplifies.

Scientists prefer to work in the regime where Da is small to limit the effects of transport; we produced an ERC solution which is accurate to $O(\mathrm{Da}^2)$. In the more complicated case where Da is moderate, we can obtain only a short-time solution analytically. Both association and dissociation experiments were considered.

In simplified form, the steric hindrance effect is encapsulated in the parameter p, which measures the ratio of the occluded areas of ligand to receptor. Though the effect can most easily be seen in Eq. (21), the parameter p propagates throughout our solutions. The dependence of p on d_l is quadratic while the dependence on R_T is linear, and hence d_l is the dominant factor in determining whether or not blocking will occur.

The wide range of p values illustrated in the Appendix shows that steric hindrance effects cannot be eliminated simply by increasing the spacing between receptors. Since R_T must be kept at a relatively high level to distinguish the BIAcore signal from experimental noise, there are ligand molecules that will remain larger than any feasible spacing.

If such effects cannot be obviated, how may they be minimized? First, as mentioned above, reducing R_T (and hence increasing the receptor spacing d_r) will reduce p, and thus the *absolute* steric hindrance effect. The *relative* size of the steric hindrance effect may be reduced by increasing K, as seen in Eq. (21). Since K is the ratio of the true affinity constant $\tilde{K}$ to C_u, it may be increased by decreasing C_u.

Many BIAcore experiments use a dextran gel as the reaction zone. The three-dimensional effects this introduces are only complicated by the fact that d_l can be of the same size as the gel thickness [6]. Such a model will necessarily be more involved, and is the object of further research.

Nomenclature

Variables and parameters

Units are listed in terms of length (L), mass (M), moles (N), or time (T). If the same letter appears both with and without tildes, the letter with a tilde has dimensions, while the letter without a tilde is dimensionless. The equation where a quantity first appears is listed, if appropriate.

$\tilde{B}(\cdot, \tilde{t})$: bound ligand concentration at position and time $\tilde{t}$, units N/L^2 (2).

$\tilde{C}(\tilde{x}, \tilde{y}, \tilde{t})$: unbound ligand concentration at position $(\tilde{x}, \tilde{y})$ and time $\tilde{t}$, units N/L^3 (2).

$\tilde{D}$: molecular diffusion coefficient, units L^2/T (9b).

d: spacing between molecules, units L.

Da: the Damköhler number, which measures the ratio of reaction and diffusion effects, dimensionless (9b).

H: height of flow channel, units L.
$h(x)$: function used in effective rate constant solution (24).
$\mathcal{I}[\beta; x]$: integration operator, defined in Eq. (37) as

$$\mathcal{I}[\beta; x] \equiv \int_0^x \beta(x')\,\mathrm{d}x'.$$

$\tilde{K}$: affinity constant, units N/L^3 (1).
$\tilde{k}_\mathrm{d}$: dissociation rate, units T^{-1} (1).
$\tilde{k}_\mathrm{a}$: association rate, units $L^3/(NT)$ (1).
L: length of the channel, units L (2).
N: Avogadro's number, units N^{-1}.
$P(\cdot,\cdot)$: normalized lower incomplete gamma function (40b).
p: area ratio of ligand to receptor molecule (12).
Pe: Peclét number for the system (9c).
R_T: receptor sites, units N/L^2 (2).
$\mathcal{S}[\cdot]$: steric hindrance operator (3).
S: slope of sensogram data for small time, units T^{-1} (38).
$\tilde{t}$: time, units T (2).
V: characteristic flow velocity, units L/T (9c).
w: width of channel, units L.
$\tilde{x}$: length along the channel, units L (2).
$\tilde{y}$: height above reacting surface, units L (9a).
$\mathcal{Z}$: the integers.
$\tilde{z}$: distance perpendicular to flow, units L.
α: dimensionless constant, defined as $K + p$ (20a).
$\beta(x)$: term in expansion of $B(x,t)$ for small t (35).
$\Gamma(\cdot)$: complete gamma function (17).
δ: ratio of ligand radius to length of channel (7b).
ϵ: aspect ratio of cross section.
ν: dimensionless parameter in moderate Da case (40a).
χ: dimensionless constant, value $1 - \alpha B_\mathrm{i}$ (25).

Other notation

a: as a subscript on ν, used to indicate the association experiment (40a).
d: as a subscript on ν, used to indicate the dissociation experiment (44b).
i: as a subscript, used to indicate an initial condition (16).
l: as a subscript, used to indicate the ligand.
max: as a subscript, used to indicate the right endpoint of the scanning range (4).
min: as a subscript, used to indicate the left endpoint of the scanning range (4).
$n \in \mathcal{Z}$: as a subscript, used to indicate a normalization factor (5) or an expansion (19).
r: as a subscript, used to indicate the receptor.

s: as a subscript, used to indicate the steady state.
u: as a subscript on C, used to indicate a characteristic value (9a).
$\bar{\ }$: used to denote the BIAcore signal, which is the mean of the bound concentration (4).
$'$: used to indicate a dummy variable (5).

Appendix

We conclude by discussing the calculation of certain parameters useful for our analysis. Using the value of H from Table 2 and the value of w from Table 3, we have that

$$\epsilon = \frac{H}{w} = 0.1, \tag{50}$$

and hence we are justified in taking it to be a small parameter in Sect. 2.2.

To calculate an upper bound for the parameter δ, we use the value of d_l from [31] cited in Table 3, as well as the value of L cited in Table 2 to obtain

$$\delta = \frac{d_\mathrm{l}}{L} = 2.08 \times 10^{-4}. \tag{51}$$

Therefore, as modeled, we are always in the small-δ limit.

Lastly, we examine the quantity $d_\mathrm{l}^2 N R_\mathrm{T}$ (which is equal to p if it is greater than 1) in various experimental cases. Using the relatively small value for R_T from [31] cited in Table 3, we have the following range:

$$2.06 \times 10^{-2} \leq d_\mathrm{l}^2 N R_\mathrm{T} \leq 9.79 \times 10^{1}, \tag{52a}$$

where we have used the extremal values of d_l cited in Table 3. If instead we use the range of values for R_T given in [30], we have

$$7.94 \times 10^{-2} \leq d_\mathrm{l}^2 N R_\mathrm{T} \leq 6.02 \times 10^{3}. \tag{52b}$$

Table 3 Parameter values from the literature. Note that d_l is a *diameter*, while most papers quote the Stokes *radius*

Reference	Parameter		
	d_l (10^{-6} cm)	R_T (10^{-12} mol/cm^2)	w (10^{-2} cm)
[2]			5
[3]	0.4		
[4]	0.726–1.19		
[23]	2.9		
[30]		0.25–4	
[31]	50	0.065	
[32]	1–1.24		

References

1. Basmadjian, D.: The effect of flow and mass transport in thrombogenesis. Ann. Biomed. Eng. **18**, 685–709 (1990)
2. BIAcore, Inc. BIAcoreSystem Manual Version 1.1. BIAcore, Inc., Uppsala, undated
3. Curto, L.M., Caramelo, J.J., Delfino, J.M.: $\Delta 98\Delta$, a functional all-β-sheet abridged form of intestinal fatty acid binding protein. Biochemistry **44**, 13847–13857 (2005)
4. Dionne, K.E., Cain, B.M., Li, R.H., Bell, W.J., Doherty, E.J., Rein, D.H., Lysaght, M.J., Gentile, F.T.: Transport characterization of membranes for immunoisolation. Biomaterials **17**, 257–266 (1996)
5. Edwards, D.A.: Estimating rate constants in a convection-diffusion system with a boundary reaction. IMA J. Appl. Math. **63**, 89–112 (1999)
6. Edwards, D.A.: The effect of a receptor layer on the measurement of rate constants. Bull. Math. Biol. **63**, 301–327 (2001)
7. Edwards, D.A.: Convection effects in the BIAcore dextran layer: surface reaction model. Bull. Math. Biol. **68**, 627–654 (2006)
8. Edwards, D.A., Goldstein, B., Cohen, D.S.: Transport effects on surface-volume biological reactions. J. Math. Biol. **39**, 533–561 (1999)
9. Edwards, D.A., Jackson, S.A.: Testing the validity of the effective rate constant approximation for surface reaction with transport. Appl. Math. Lett. **15**, 547–552 (2002)
10. Edwards, D.A., Swaminathan, S.: The effect of receptor site nonuniformity on the measurement of rate constants. Appl. Math. Lett. **18**, 1101–1107 (2005)
11. Garland, P.B.: Optical evanescent wave methods for the study of biomolecular reactions. Q. Rev. Biophys. **29**, 91–117 (1996)
12. Gherardi, E., Youles, M.E., Miguel, R.N., Blundell, T.L., Iamele, L., Gough, J., Bandyopadhyay, A., Hartmann, G., Butler, P.J.G.: Functional map and domain structure of MET, the product of the c-*met* protooncogene and receptor for hepatocyte growth factor scatter factor. PNAS **100**, 12039–12044 (2003)
13. Grabowski, E.F., Friedman, L.I., Leonard, E.F.: Effects of shear rate on the diffusion and adhesion of blood platelets to a foreign surface. Ind. Eng. Chem. Fund. **11**, 224–232 (1972)
14. He, X.Y., Li, N., Goldstein, B.: Lattice boltzmann simulation of diffusion-convection systems with surface chemical reaction. Mol. Sim. **25**, 145–156 (2000)
15. Hoffman, T.L., Canziani, G., Jia, L., Rucker, J., Doms, R.W.: A biosensor assay for studying ligand-membrane receptor interactions: binding of antibodies and HIV-1 env to chemokine receptors. Proc. NAS **97**, 11215–11220 (2000)
16. Joss, L., Morton, T.A., Doyle, M.L., Myszka, D.G.: Interpreting kinetic rate constants from optical biosensor data recorded on a decaying surface. Anal. Biochem. **261**, 203–210 (1998)
17. Karlsson, R., Fält, A.: Experimental design for kinetic analysis of protein-protein interactions with surface plasmon resonance biosensors. J. Immunol. Methods **200**, 121–133 (1997)
18. Karlsson, R., Michaelson, A., Mattson, L.: Kinetic analysis of monoclonal antibody–antigen interactions with a new biosensor based analytical system. J. Immunol. Methods **145**, 229–240 (1991)
19. Kleene, S.J.: Both external and internal calcium reduce the sensitivity of the olfactory cyclic-nucleotide-gated channel to cAMP. J. Neurophys. **81**, 2675–2682 (1999)
20. Lee, M., Rhodes, A.L., Wyatt, M.D., Forrow, S., Hartley, J.A.: GC-base sequence recognition by oligo (imidazolecarboxamide) and C-terminus-modified analogs of distamycin deduced from circular dichroism, proton nuclear magnetic resonance, and methidiumpropylethylenediaminetetraacetate-iron(II) footprinting studies. Biochemistry **32**, 4237–4245 (1993)
21. Liedberg, B., Lundstrom, I., Stenberg, E.: Principles of biosensing with an extended coupling matrix and surface-plasmon resonance. Sens. Actuators B **11**, 63–72 (1993)
22. Long, W.M., Kalachev, L.V.: Asymptotic analysis of dissolution of a spherical bubble (case of fast reaction outside the bubble). Rocky Mt. J. Math. **30**, 293–313 (2000)
23. Marshall, C.B., Chakrabartty, A., Davies, P.L.: Hyperactive antifreeze protein from winter flounder is a very long rod-like dimer of α-helices. J. Biol. Chem. **280**, 17920–17929 (2005)
24. O'Shannessy, D.J., Brigham-Burke, M., Peck, K.: Immobilization chemistries suitable for use in the BIAcore surface plasmon resonance detector. Anal. Biochem. **205**, 132–136 (1992)
25. Raghavan, M., Chen, M.Y., Gastinel, L.N., Bjorkman, P.J.: Investigation of the interaction between the class I MHC-related Fc receptor and its immunoglobulin G ligand. Immunity **1**, 303–315 (1994)
26. Staszak, K., Prochaska, K.: Estimation of diffusion coefficients based on adsorption measurements in model extraction systems. Chem. Eng. Tech. **28**, 985–990 (2005)

27. Sutovsky, H., Gazit, E.: The von Hippel-Lindau tumor suppressor protein is a molten globule under native conditions: implications for its physiological activities. J. Biol. Chem. **279**, 17190–17196 (2004)
28. Szabo, A., Stolz, L., Granzow, R.: Surface plasmon resonance and its use in bio-molecular interaction analysis (BIA). Curr. Opin. Struct. Biol. **5**, 699–705 (1995)
29. Ward, A.F.H., Tordai, L.: Time-dependence of boundary tensions of solutions i. the role of diffusion in time-effects. J. Chem. Phys. **14**, 453–461 (1946)
30. Yarmush, M.L., Patankar, D.B., Yarmush, D.M.: An analysis of transport resistance in the operation of BIAcore^{TM}; implications for kinetic studies of biospecific interactions. Mol. Immunol. **33**, 1203–1214 (1996)
31. Zheng, Y., Rundell, A.: Biosensor immunosurface engineering inspired by B-cell membrane-bound antibodies: modeling and analysis of multivalent antigen capture by immobilized antibodies. IEEE Trans. Nanobiosci. **2**, 14–25 (2003)
32. Zhou, J., Low, P.S.: Characterization of the reversible conformational equilibrium in the cytoplasmic domain of human erythrocyte membrane band 3. J. Biol. Chem. **276**, 38147–38151 (2001)